AIMS Mathematics, 9(6): 15202–15222.
DOI: 10.3934/math.2024738
Received: 08 January 2024
Revised: 11 April 2024
Accepted: 15 April 2024
Published: 26 April 2024

http://www.aimspress.com/journal/Math

Research article

Exploring unconventional optical soliton solutions for a novel q-deformed mathematical model

Khalid K. Ali[1,*] **and Weam G. Alharbi**[2]

[1] Mathematics Department, Faculty of Science, Al-Azhar University, Nasr-City, Cairo, Egypt
[2] Department of Mathematics, Faculty of Science, University of Tabuk, Tabuk 71491, Saudi Arabia

* **Correspondence:** Email: khalidkaram2012@azhar.edu.eg; Tel: +201033530861.

Abstract: This paper presents a significant contribution in the form of a new general equation, namely the q-deformed equation or the q-deformed tanh-Gordon equation. The introduction of this novel equation opens up new possibilities for modeling physical systems that exhibit violated symmetries. By employing the (G'/G) expansion method, we have successfully derived solitary wave solutions for the newly defined q-deformed equation under specific parameter regimes. These solutions provide valuable insights into the behavior of the system and its dynamics. To further validate the obtained analytical results, the numerical solution of the q-deformed equation has been constructed by using the finite difference method. This numerical approach ensures the accuracy and reliability of the findings. To facilitate a comprehensive understanding of the results, we have included two- and three-dimensional tables and figures, which provide visual representations and comparisons between the analytical and numerical solutions. These graphical illustrations enhance the clarity and interpretation of the obtained data. The significance of the q-deformation lies in its ability to model physical systems that exhibit deviations from standard symmetry properties, such as extensivity. This type of modeling is increasingly relevant in various fields, as it allows for a more accurate representation of real-world phenomena.

Keywords: new q-deformed model; optical solutions; the (G'/G)-expansion method; numerical method
Mathematics Subject Classification: 35-XX, 65-XX

1. Introduction

Dynamical models play a fundamental role in various scientific fields, although their coverage in the literature is unevenly distributed among these fields. Almusawa et al. [1] conducted a protracted study on a real physical phenomenon generated by media inhomogeneities, highlighting the importance of

dynamical models in elucidating and analyzing complex systems. Moaaz and Ramos [2] introduced a new precise criterion for oscillation in second-order Emden-Fowler neutral differential equations, further emphasizing the significance of dynamical models in capturing and predicting system behavior. Building on this, Moaaz et al. [3] presented new oscillation results for fourth-order neutral differential equations, contributing to the comprehensive understanding of dynamical systems. Ahmad et al. [4] focused on the global stability of a fractional order HIV/AIDS epidemic model, showcasing the application of dynamical models in the study of real-world phenomena and as a tool to inform computational modeling efforts. They constitute a crucial area of research in mathematics and theoretical physics, often relying on nonlinear ordinary or partial differential equations. Nonlinearity has enabled the study of significant effects and phenomena, not only in macroscopic systems but also in microscopic systems governed by quantum physics. An example of such phenomena is the occurrence of Rogue waves [5, 6]. Incorporating the q-deformed hyperbolic function as introduced by Arai in the 1990s [7, 8], into a dynamical system disrupts the symmetry of the system and consequently affects the symmetry of the solution. Recently, numerous solutions have been derived for the Schrödinger equation and Dirac equation and they entail employing the q-deformed hyperbolic potential [9, 10]. The use of q-deformed functions shows great promise for applications involving modeling atom-trapping potentials or statistical distributions in Bose-Einstein condensates [11], as well as exploring the vibrational spectra of diatomic molecules [12,13]. The study of q-deformed equations has led to the development of various techniques and tools, including q-special functions, q-difference equations, and q-integral transforms. These tools have proven to be useful in the study of a wide range of problems in mathematics and physics.

The generalized q-deformed sinh-Gordon equation, an extension of the sinh-Gordon equation, was introduced by H. Eleuch in 2018 in the following form [14]:

$$\frac{\partial^2 u(x,t)}{\partial x^2} - \frac{\partial^2 u(x,t)}{\partial t^2} = [\sinh_{\mathfrak{q}}(u^{\gamma})]^p - \delta, \quad t \geqslant 0, \quad 0 < \mathfrak{q} \leqslant 1, \tag{1.1}$$

where $\sinh_{\mathfrak{q}}$ is defined by:

$$\sinh_{\mathfrak{q}}(t) = \frac{e^t - \mathfrak{q}e^{-t}}{2},$$

and $\cosh_{\mathfrak{q}}$ is defined by:

$$\cosh_q(t) = \frac{e^t + \mathfrak{q}e^{-t}}{2}.$$

Eleuch proposed an analysis of the propagating wave solutions for this more comprehensive form of the equation.

Many researchers have conducted both analytical and numerical studies (1.1) [14–17].
A new form of the q-deformed Sinh-Gordon equation was introduced by Ali et al. in 2023 [18]:

$$\frac{\partial^2 u(x,t)}{\partial x^2} - \frac{\partial^2 u(x,t)}{\partial t^2} = e^{\alpha u}[\sinh_{\mathfrak{q}}(u^{\gamma})]^p - \delta. \tag{1.2}$$

In this work, a new form of the q-deformed equation is introduced as follows:

$$\frac{\partial^2 u(x,t)}{\partial x^2} - \frac{\partial^2 u(x,t)}{\partial t^2} = \left(\tanh_{\mathfrak{q}} u(x,t)^{\varrho}\right)^p \left(e^{\lambda u(x,t)} + \beta\mathfrak{q}\right)^{\rho} - \delta, \tag{1.3}$$

where $\tanh_{\mathfrak{q}}$ is defined by:

$$\tanh_{\mathfrak{q}}(t) = \frac{e^t - \mathfrak{q}e^{-t}}{e^t + \mathfrak{q}e^{-t}},$$

where $u(x,t)$ is a scalar field, $\tanh_{\mathfrak{q}}$ denotes the $\mathfrak{q}$-tanh function, ϱ, p, λ, β, and ρ are constants, and δ is a source term. This equation is a generalization of the standard $\mathfrak{q}$-deformed equation and can be applied to a rich variety of nonlinear phenomena and complex dynamics.

In this paper, we present an extended study for a new form of the $\mathfrak{q}$-deformed equation. To date this equation has not been presented in this form. We first use the (G'/G)-expansion method to derive exact analytical solutions for the equation [19]. In addition, we introduce a numerical scheme by using the finite difference method to obtain numerical solutions for the equation and compare them with the analytical solutions [20, 21]. We also study the behavior of the solutions under various parameter regimes, including the effects of the deformation parameter $\mathfrak{q}$.

This paper is organized into several sections. The second section contains an analysis of the proposed equation. The third section describes the analytical methodology that was used in this study. The fourth section presents the analytical solutions that were obtained. The fifth section provides numerical solutions. The sixth section includes graphical representations of the solutions that were obtained. In the seventh section, we analyze and discuss the results that were obtained. Finally, in the eighth section, we present our conclusions based on the work that was conducted in this study.

2. The mathematical analysis of the model

To obtain the traveling wave solution of Eq (1.3), we employ the following transformation:

$$u(x,t) = v(\mathcal{E}), \tag{2.1}$$

where

$$\mathcal{E} = kx - \vartheta t, \tag{2.2}$$

where, ϑ represents the speed of the traveling wave. With the help of Eqs (2.1) and (2.2), we can rewrite Eq (1.3) as:

$$\left(k^2 - \vartheta^2\right) v''(\mathcal{E}) - \tanh_q \left(v(\mathcal{E})^{\varrho}\right)^p \left(e^{\lambda v(\mathcal{E})} + \beta q\right)^{\rho} + \delta = 0. \tag{2.3}$$

Now we will look at two cases for Eq (2.3).

- **Case 1:** $\lambda = 2, \varrho = p = 1, \delta = -q, \beta = 1, \rho = 1$.

Thus, Eq (2.3) can be written as:

$$\left(k^2 - \vartheta^2\right) v''(\mathcal{E}) - \left(e^{2v(\mathcal{E})}\right) = 0. \tag{2.4}$$

We can multiply both sides of Eq (2.4) by $v'(\mathcal{E})$ and get the following equation after integration,

$$\frac{1}{2}\left(-\left(\left(\vartheta^2 - k^2\right) v'(\mathcal{E})^2\right) - e^{2v(\mathcal{E})}\right) - C_1 = 0. \tag{2.5}$$

The integration constant is C_1.
Let

$$v(\mathcal{E}) = \frac{1}{2} ln(h(\mathcal{E})). \tag{2.6}$$

Then, Eq (2.5) becomes,

$$-8C_1h(\mathcal{E})^2+\left(k^2-\vartheta^2\right)h'(\mathcal{E})^2-4h(\mathcal{E})^3=0. \tag{2.7}$$

Therefore, we can solve Eq (2.7) to obtain the solution of Eq (1.3) in the first case.

- **Case 2:** Assume that $\lambda=2,\varrho=1,p=2,\rho=2,\beta=1,\delta=q^2$.

Then, Eq (2.3) can be written as:

$$\left(k^2-\vartheta^2\right)v''(\mathcal{E})+2qe^{2v(\mathcal{E})}-e^{4v(\mathcal{E})}=0. \tag{2.8}$$

We can multiply both sides of Eq (2.8) by $v'(\mathcal{E})$ and get the following equation after integration.

$$-\frac{1}{2}\left(\vartheta^2-k^2\right)v'(\mathcal{E})^2+qe^{2v(\mathcal{E})}-\frac{1}{4}e^{4v(\mathcal{E})}-C_2=0. \tag{2.9}$$

Let

$$v(\mathcal{E})=ln(h(\mathcal{E})). \tag{2.10}$$

Then, Eq (2.9) becomes,

$$-4C_2h(\mathcal{E})^2+2(k^2-\vartheta^2)h'(\mathcal{E})^2+4qh(\mathcal{E})^4-h(\mathcal{E})^6=0. \tag{2.11}$$

Then, we can solve Eq (2.11) to find the solution Eq (1.3) in the second case.

3. The strategy of the (G'/G)-expansion approach

We can express the governing equation in the following manner:

$$F(u,u_{xx},u_{tt},...)=0. \tag{3.1}$$

Equation (3.1) features a polynomial function F that depends on the function u and its derivatives with respect to both space and time. To convert this partial differential equation into an ordinary differential equation, we can utilize the traveling wave transformation Eq (2.1):

$$H(v,v'',...)=0. \tag{3.2}$$

The essential steps of the (G'/G)-expansion method are as follows:

Step 1: Let us assume that the exact solutions to Eq (3.2) can be expressed as follows:

$$v(\mathcal{E})=\sum_{i=0}^{N}R_i\left(\frac{G'}{G}\right)^i, \tag{3.3}$$

where, $G=G(\mathcal{E})$ satisfies the second-order linear ordinary differential equation given by:

$$G''(\mathcal{E})+\sigma G'(\mathcal{E})+\nu G(\mathcal{E})=0, \tag{3.4}$$

where $R_i\ \ (i=0,1,2,...,N),R_N\neq 0,\ \ \sigma$ and ν are constants to be calculated.

Step 2: Equation (3.2) contains a highest order derivative term and the highest power nonlinear term. By balancing these two terms, a positive integer N can be obtained, as shown in Eq (3.3). This integer value is likely to be significant in the characterization of the behavior of the system described by the equations, although further information about the equations is necessary to fully understand the meaning of N.

Step 3: We can identify three distinct families of traveling wave solutions for Eq (3.4):

Family 1: Hyperbolic function solutions, when $\sigma^2 - 4\nu > 0$,

$$\frac{G'}{G} = \frac{-\sigma}{2} + \frac{1}{2}\sqrt{\sigma^2 - 4\nu}\frac{g_1 \sinh \frac{1}{2}\sqrt{\sigma^2 - 4\nu}\mathcal{E} + g_2 \cosh \frac{1}{2}\sqrt{\sigma^2 - 4\nu}\mathcal{E}}{g_1 \cosh \frac{1}{2}\sqrt{\sigma^2 - 4\nu}\mathcal{E} + g_2 \sinh \frac{1}{2}\sqrt{\sigma^2 - 4\nu}\mathcal{E}}. \tag{3.5}$$

Family 2: Trigonometric function solutions, when $\sigma^2 - 4\nu < 0$,

$$\frac{G'}{G} = \frac{-\sigma}{2} + \frac{1}{2}\sqrt{4\nu - \sigma^2}\frac{-g_1 \sin \frac{1}{2}\sqrt{4\nu - \sigma^2}\mathcal{E} + g_2 \cos \frac{1}{2}\sqrt{4\nu - \sigma^2}\mathcal{E}}{g_1 \cos \frac{1}{2}\sqrt{4\nu - \sigma^2}\mathcal{E} + g_2 \sin \frac{1}{2}\sqrt{4\nu - \sigma^2}\mathcal{E}}. \tag{3.6}$$

Family 3: Rational function solutions, when $\sigma^2 - 4\nu = 0$,

$$\frac{G'}{G} = \frac{-\sigma}{2} + \frac{g_2}{g_1 + g_2\mathcal{E}}. \tag{3.7}$$

Step 4: To derive a system of algebraic equations with R_i, k, and ϑ, we substitute Eq (3.3) for Eq (3.2) and utilize Eq (3.4) to group together the terms with identical powers of $(\frac{G'}{G})$. We then equate each coefficient to zero, and this system of equations can be solved by using the Mathematica program.

4. The model's mathematical solutions

In this section, we use the (G'/G)-expansion method to determine the analytical solutions for the two cases considered in the problem given by Eq (1.3). The (G'/G)-expansion method is a highly effective analytical technique that is utilized to obtain approximate solutions to nonlinear differential equations.

- **The analytical solution of case one with $\lambda = 2, \varrho = p = 1, \delta = -q, \beta = 1, \rho = 1$**:

Applying the balance principle to Eq (2.7) between the terms h'^2 and h^3 yields $2N + 2 = 3N$, which implies that $N = 2$. Using Eq (3.3), we can express the solution to Eq (2.7) as follows:

$$h(\mathcal{E}) = \sum_{i=0}^{2} R_i \left(\frac{G'}{G}\right)^i. \tag{4.1}$$

By substituting Eq (4.1) for Eq (2.7) and equating the coefficients of like powers of $\left(\frac{G'}{G}\right)$ to zero, we obtain the following system:

$$-8C_1R_0^2 + k^2\nu^2R_1^2 - \nu^2R_1^2\vartheta^2 - 4R_0^3 = 0,$$

$$-16C_1R_0R_1 + 4k^2\nu^2R_1R_2 + 2k^2\nu R_1^2\sigma - 4\nu^2R_1R_2\vartheta^2 - 2\nu R_1^2\sigma\vartheta^2 - 12R_0^2R_1 = 0,$$
$$-8C_1R_1^2 - 16C_1R_0R_2 + 4k^2\nu^2R_2^2 + 8k^2\nu R_1R_2\sigma + 2k^2\nu R_1^2 + k^2R_1^2\sigma^2$$
$$-4\nu^2R_2^2\vartheta^2 - 8\nu R_1R_2\sigma\vartheta^2 - 2\nu R_1^2\vartheta^2 - R_1^2\sigma^2\vartheta^2 - 12R_0R_1^2 - 12R_0^2R_2 = 0,$$
$$-16C_1R_2R_1 + 8k^2\nu R_2^2\sigma + 8k^2\nu R_2R_1 + 4k^2R_2R_1\sigma^2 + 2k^2R_1^2\sigma - 8\nu R_2^2\sigma\vartheta^2$$
$$-8\nu R_2R_1\vartheta^2 - 4R_2R_1\sigma^2\vartheta^2 - 2R_1^2\sigma\vartheta^2 - 4R_1^3 - 24R_0R_2R_1 = 0,$$
$$-8C_1R_2^2 + 8k^2\nu R_2^2 + 4k^2R_2^2\sigma^2 + 8k^2R_1R_2\sigma + k^2R_1^2 - 8\nu R_2^2\vartheta^2$$
$$-4R_2^2\sigma^2\vartheta^2 - 8R_1R_2\sigma\vartheta^2 - R_1^2\vartheta^2 - 12R_0R_2^2 - 12R_1^2R_2 = 0,$$
$$8k^2R_2^2\sigma + 4k^2R_1R_2 - 8R_2^2\sigma\vartheta^2 - 4R_1R_2\vartheta^2 - 12R_1R_2^2 = 0,$$
$$4k^2R_2^2 - 4R_2^2\vartheta^2 - 4R_2^3 = 0.$$

By solving the aforementioned set of equations using the Mathematica program, the following sets of solutions were obtained:

$$R_0 = \frac{\nu R_1}{\sigma},\ R_2 = \frac{R_1}{\sigma},\ C_1 = \frac{R_1\sigma^2 - 4\nu R_1}{8\sigma},\ k = \mp\frac{\sqrt{R_1 + \sigma\vartheta^2}}{\sqrt{\sigma}}. \tag{4.2}$$

By plugging the values from Eq (4.2) into Eq (4.1) and utilizing Eqs (3.6) and (3.5), we can determine $h(\mathcal{E})$. Subsequently, by substituting $h(\mathcal{E})$ into Eq (2.6), we can find $v(\mathcal{E})$. Finally, by replacing $v(\mathcal{E})$ in Eq (2.1) along with Eq (2.2), we can obtain the solutions of Eq (1.3) when $\lambda = 2, \varrho = p = 1, \delta = -q, \beta = 1, \rho = 1$ as follows:

Family 1: Hyperbolic function solutions, when $\sigma^2 - 4\nu > 0$,

$$\begin{aligned} u_{1,2}(x,t) = {} & \frac{1}{2}ln\Big(R_0 + \\ & R_1\Big(\frac{-\sigma}{2} + \frac{1}{2}\sqrt{\sigma^2 - 4\nu}\frac{g_1\sinh\frac{1}{2}\sqrt{\sigma^2 - 4\nu}(kx - \vartheta t) + g_2\cosh\frac{1}{2}\sqrt{\sigma^2 - 4\nu}(kx - \vartheta t)}{g_1\cosh\frac{1}{2}\sqrt{\sigma^2 - 4\nu}(kx - \vartheta t) + g_2\sinh\frac{1}{2}\sqrt{\sigma^2 - 4\nu}(kx - \vartheta t)}\Big) + \\ & R_2\Big(\frac{-\sigma}{2} + \frac{1}{2}\sqrt{\sigma^2 - 4\nu}\frac{g_1\sinh\frac{1}{2}\sqrt{\sigma^2 - 4\nu}(kx - \vartheta t) + g_2\cosh\frac{1}{2}\sqrt{\sigma^2 - 4\nu}(kx - \vartheta t)}{g_1\cosh\frac{1}{2}\sqrt{\sigma^2 - 4\nu}(kx - \vartheta t) + g_2\sinh\frac{1}{2}\sqrt{\sigma^2 - 4\nu}(kx - \vartheta t)}\Big)^2\Big). \end{aligned} \tag{4.3}$$

Family 2: Trigonometric function solutions, when $\sigma^2 - 4\nu < 0$,

$$\begin{aligned} u_{3,4}(x,t) = {} & \frac{1}{2}ln\Big(R_0 + \\ & R_1\Big(\frac{-\sigma}{2} + \frac{1}{2}\sqrt{\sigma^2 - 4\nu}\frac{-g_1\sin\frac{1}{2}\sqrt{\sigma^2 - 4\nu}(kx - \vartheta t) + g_2\cos\frac{1}{2}\sqrt{\sigma^2 - 4\nu}(kx - \vartheta t)}{g_1\cos\frac{1}{2}\sqrt{\sigma^2 - 4\nu}(kx - \vartheta t) + g_2\sin\frac{1}{2}\sqrt{\sigma^2 - 4\nu}(kx - \vartheta t)}\Big) + \\ & R_2\Big(\frac{-\sigma}{2} + \frac{1}{2}\sqrt{\sigma^2 - 4\nu}\frac{-g_1\sin\frac{1}{2}\sqrt{\sigma^2 - 4\nu}(kx - \vartheta t) + g_2\cos\frac{1}{2}\sqrt{\sigma^2 - 4\nu}(kx - \vartheta t)}{g_1\cos\frac{1}{2}\sqrt{\sigma^2 - 4\nu}(kx - \vartheta t) + g_2\sin\frac{1}{2}\sqrt{\sigma^2 - 4\nu}(kx - \vartheta t)}\Big)^2\Big). \end{aligned} \tag{4.4}$$

- **The analytical solution of case two with $\lambda = 2, \varrho = 1; p = 2, \rho = 2, \beta = 1, \delta = q^2$**:

By applying the balance principle to Eq (2.11) between the terms h'^2 and h^6, we arrive at $2N+2=6N$. However, this equation does not produce a solution for N. As a result, we must make a transformation as follows:

$$h(\mathcal{E}) = \sqrt{f(\mathcal{E})}. \tag{4.5}$$

Then, Eq (2.11) becomes

$$(k-\vartheta)(k+\vartheta)f'(\mathcal{E})^2 - 2f(\mathcal{E})^2\left(4C_2 - 4qf(\mathcal{E}) + f(\mathcal{E})^2\right) = 0. \tag{4.6}$$

Applying the balance principle to Eq (4.6) between the terms f'^2 and f^4 yields $2N+2=4N$, which implies that $N=1$. From Eq (3.3), the solution of Eq (4.6) can be presented as follows:

$$f(\mathcal{E}) = \sum_{i=0}^{1} R_i\left(\frac{G'}{G}\right)^i. \tag{4.7}$$

By substituting Eq (4.7) into Eq (4.6) and equating the coefficients of like powers of $\left(\frac{G'}{G}\right)$ to zero, we obtain the following system:

$$-8C_2R_0^2 + k^2\nu^2R_1^2 + 8qR_0^3 - \nu^2R_1^2\vartheta^2 - 2R_0^4 = 0,$$

$$-16C_2R_1R_0 + 2k^2\nu R_1^2\sigma + 24qR_1R_0^2 - 2\nu R_1^2\sigma\vartheta^2 - 8R_1R_0^3 = 0,$$

$$-8C_2R_1^2 + 2k^2\nu R_1^2 + k^2R_1^2\sigma^2 + 24qR_0R_1^2 - 2\nu R_1^2\vartheta^2 - R_1^2\sigma^2\vartheta^2 - 12R_0^2R_1^2 = 0,$$

$$2k^2R_1^2\sigma + 8qR_1^3 - 2R_1^2\sigma\vartheta^2 - 8R_0R_1^3 = 0,$$

$$k^2R_1^2 - R_1^2\vartheta^2 - 2R_1^4 = 0.$$

By using the Mathematica program to solve the aforementioned set of equations, we obtained the following sets of solutions:

- **Set 1:**

$$R_0 = \frac{q^2\sigma^2}{\sqrt{q^2\sigma^2\left(\sigma^2-4\nu\right)}} + q,\quad R_1 = \frac{2q^2\sigma}{\sqrt{q^2\sigma^2\left(\sigma^2-4\nu\right)}}, C_2 = q^2,\quad \vartheta = \mp\frac{\sqrt{\nu^2q\left(k^2-\frac{8q^2}{\sigma^2-4\nu}\right)}}{\nu\sqrt{q}}. \tag{4.8}$$

By substituting the values from Eq (4.8) into Eq (4.7), we obtain $f(\mathcal{E})$. Then, by substituting $f(\mathcal{E})$ into Eq (4.5) and utilizing Eqs (3.6) and (3.5), we can determine $h(\mathcal{E})$. Next, by substituting $h(\mathcal{E})$ into Eq (2.10), we can find $v(\mathcal{E})$. Finally, by replacing $v(\mathcal{E})$ in Eq (2.1) along with Eq (2.2), we can obtain the solutions of Eq (1.3) when $\lambda=2, \varrho=1; p=2, \rho=2, \beta=1, \delta=q^2$ as follows:

Family 1: Hyperbolic function solutions, when $\sigma^2-4\nu>0$,

$$u_{1,2}(x,t) = ln\Big(R_0+ R_1\Big(\frac{-\sigma}{2} + \frac{1}{2}\sqrt{\sigma^2-4\nu}\frac{g_1\sinh\frac{1}{2}\sqrt{\sigma^2-4\nu}(kx-\vartheta t) + g_2\cosh\frac{1}{2}\sqrt{\sigma^2-4\nu}(kx-\vartheta t)}{g_1\cosh\frac{1}{2}\sqrt{\sigma^2-4\nu}(kx-\vartheta t) + g_2\sinh\frac{1}{2}\sqrt{\sigma^2-4\nu}(kx-\vartheta t)}\Big)\Big)^{\frac{1}{2}}. \tag{4.9}$$

Family 2: Trigonometric function solutions, when $\sigma^2 - 4\nu < 0$,

$$u_{3,4}(x,t) = ln\Big(R_0 + R_1\Big(\frac{-\sigma}{2} + \frac{1}{2}\sqrt{\sigma^2-4\nu}\frac{-g_1\sin\frac{1}{2}\sqrt{\sigma^2-4\nu}(kx-\vartheta t) + g_2\cos\frac{1}{2}\sqrt{\sigma^2-4\nu}(kx-\vartheta t)}{g_1\cos\frac{1}{2}\sqrt{\sigma^2-4\nu}(kx-\vartheta t) + g_2\sin\frac{1}{2}\sqrt{\sigma^2-4\nu}(kx-\vartheta t)}\Big)\Big)^{\frac{1}{2}}. \tag{4.10}$$

- **Set 2:**

$$R_0 = q - \frac{q^2\sigma^2}{\sqrt{q^2\sigma^2(\sigma^2-4\nu)}},\ R_1 = -\frac{2q^2\sigma}{\sqrt{q^2\sigma^2(\sigma^2-4\nu)}}, C_2 = q^2, \vartheta = \mp\frac{\sqrt{\nu^2 q\left(k^2 - \frac{8q^2}{\sigma^2-4\nu}\right)}}{\nu\sqrt{q}}. \tag{4.11}$$

By substituting the values from Eq (4.11) into Eq (4.7), we obtain $f(\mathcal{E})$. Then, by substituting $f(\mathcal{E})$ into Eq (4.5) and utilizing Eqs (3.6) and (3.5), we can determine $h(\mathcal{E})$. Next, by substituting $h(\mathcal{E})$ into Eq (2.10), we can find $v(\mathcal{E})$. Finally, by replacing $v(\mathcal{E})$ in Eq (2.1) along with Eq (2.2), we can obtain the solutions of Eq (1.3) when $\lambda = 2, \varrho = 1, p = 2, \rho = 2, \beta = 1, \delta = q^2$ as follows:

Family 1: Hyperbolic function solutions, when $\sigma^2 - 4\nu > 0$,

$$u_{5,6}(x,t) = ln\Big(R_0 + R_1\Big(\frac{-\sigma}{2} + \frac{1}{2}\sqrt{\sigma^2-4\nu}\frac{g_1\sinh\frac{1}{2}\sqrt{\sigma^2-4\nu}(kx-\vartheta t) + g_2\cosh\frac{1}{2}\sqrt{\sigma^2-4\nu}(kx-\vartheta t)}{g_1\cosh\frac{1}{2}\sqrt{\sigma^2-4\nu}(kx-\vartheta t) + g_2\sinh\frac{1}{2}\sqrt{\sigma^2-4\nu}(kx-\vartheta t)}\Big)\Big)^{\frac{1}{2}}. \tag{4.12}$$

Family 2: Trigonometric function solutions, when $\sigma^2 - 4\nu < 0$,

$$u_{7,8}(x,t) = ln\Big(R_0 + R_1\Big(\frac{-\sigma}{2} + \frac{1}{2}\sqrt{\sigma^2-4\nu}\frac{-g_1\sin\frac{1}{2}\sqrt{\sigma^2-4\nu}(kx-\vartheta t) + g_2\cos\frac{1}{2}\sqrt{\sigma^2-4\nu}(kx-\vartheta t)}{g_1\cos\frac{1}{2}\sqrt{\sigma^2-4\nu}(kx-\vartheta t) + g_2\sin\frac{1}{2}\sqrt{\sigma^2-4\nu}(kx-\vartheta t)}\Big)\Big)^{\frac{1}{2}}. \tag{4.13}$$

5. The numerical solution for the model

In this section, we employ approximations for both spatial x and temporal t derivatives, as detailed in prior studies [20, 21].

The purpose of these approximations is to estimate the time derivative of the exact solution at a specific grid point, as based on the numerical solution at that point and its neighboring points. The accuracy of these approximations is determined by both the order of the approximation and the spacing between the grid points. Generally, using higher order approximations and smaller grid spacings results in more accurate estimates of the time derivative.

Assuming that u represents the exact solution at the grid point (x_i, t_n) and U represents the numerical solution at the same point, we can express the approximation for the space derivative with respect to x as follows:

$$u_{xx} \simeq \frac{1}{(\Delta x)^2}\Big(U_{i+1,n} - 2U_{i,n} + U_{i-1,n}\Big). \tag{5.1}$$

The following equation is the approximation for the time derivative with respect to t:

$$u_{tt} \simeq \frac{U_{i,n+1} - 2U_{i,n} + U_{i,n-1}}{(\Delta t)^2}. \tag{5.2}$$

Upon substituting Eqs (5.1) and (5.2) into Eq (1.3), we obtain a system of difference equations at $U_{i,n}$,

$$\begin{aligned} &\frac{1}{(\Delta x)^2}\Big(U_{i+1,n} - 2U_{i,n} + U_{i-1,n}\Big) - \frac{U_{i,n+1} - 2U_{i,n} + U_{i,n-1}}{(\Delta t)^2} \\ &= \left(\tanh_{\mathfrak{q}} U_{i,n}^{\varrho}\right)^{p} \left(e^{\lambda U_{i,n}} + \beta \mathfrak{q}\right)^{\rho} - \delta, \quad i = 0, 1, ..., N, \quad n = 1, 2, ..., M. \end{aligned} \tag{5.3}$$

The system described above consists of $(N + 1)$ equations with $(N + 3)$ unknowns at each time level n. By utilizing Eq (5.3) and applying the boundary conditions obtained from the analytical solutions, we can solve the system numerically by using a Mathematica program on a PC with "Core i7-1165G7 @ 2.80GHz". If we substitute $n = 0, 1, ..., M$, we obtain a system of algebraic equations involving the levels $U^{-1}, U^0, ..., U^{m+1}$. However, since U^{-1} is a delayed value that we do not know, we must start with $n = 1, ..., M$. To solve the system, we need to determine the initial values U^0 and U^1, which can be obtained from the analytical solution. To study the convergence of the solutions to ensure the accuracy of the proposed method, we can calculate L_2 and L_∞ as follows:

$$\begin{aligned} L_2 &= \sqrt{\Delta x \sum_{i=0}^{N} |U_{Num.} - u_{Ex.}|^2}, \\ L_\infty &= \underset{0 \le i \le N}{\text{Max}} |U_{Num.} - u_{Ex.}|. \end{aligned}$$

The numerical results

In this section, we provide numerical outcomes for the $\mathfrak{q}$-deformed tanh-Gordon equation's general form. To accomplish this, we will examine two particular instances of the generalized $\mathfrak{q}$-deformed tanh-Gordon equation:

- **The numerical results for case one: $\lambda = 2, \varrho = p = 1, \delta = -q, \beta = 1, \rho = 1$**

Table 1 and Figure 7 present a comparison between the numerical results obtained from our numerical scheme and the analytical solution given by Eq (4.3) for Eq (1.3) with the following parameter values: $g_1 = 0.2, g_2 = 0.01, \nu = 0.001, q = 0.1, R_1 = 0.1, \sigma = 0.2, \vartheta = 0.1, \Delta t = 0.1, \Delta x = 0.2, -10 \leqslant x \leqslant 10$, and $t = 5$. These comparisons demonstrate the accuracy of our numerical scheme and the validity of our analytical solutions, as indicated by the close agreement between the numerical and analytical results.

Table 1. Comparison between the numerical results obtained via our numerical scheme and the analytical solution.

x	Numerical solution	Analytical solution	Absolute error
-10	3.31053	3.31053	0.00000
-8	3.24612	3.24612	4.61672×10^{-7}
-6	3.19420	3.19420	9.19299×10^{-7}
-4	3.15609	3.15609	1.31071×10^{-6}
4	3.15729	3.15729	1.13184×10^{-6}
6	3.19595	3.19595	7.14930×10^{-6}
8	3.24838	3.24838	3.28793×10^{-7}
10	3.31323	3.31323	0.00000

The results presented in Table 1 and Figure 7 provide valuable insights into the behavior and properties of the solutions for Eq (1.3) under the specified parameter values. Moreover, these comparisons demonstrate the effectiveness of our combined analytical and numerical approach in investigating the equations we derived; they aslo provide evidence of the accuracy and reliability of our numerical and analytical solutions.

Table 2 and Figure 8 present the numerical results alongside the analytical solution Eq (4.4) for Eq (1.3) with the following parameter values: $g_1 = 0.1, g_2 = 0.0001, \nu = 0.01, q = 0.1, R_1 = 0.001, \sigma = 0.001, \vartheta = 0.4, \Delta t = 0.1, \Delta x = 0.2, -10 \leqslant x \leqslant 10$ and $t = 5$.

Table 2. Comparison between the numerical results obtained via our numerical scheme and the analytical solution.

x	Numerical solution	Analytical solution	Absolute error
-10	1.05993	1.05993	0.00000
-8	1.58215	1.58227	1.20778×10^{-4}
-6	1.89013	1.89022	9.23073×10^{-4}
-4	2.08808	2.08812	3.84487×10^{-5}
4	2.27593	2.27596	2.53936×10^{-5}
6	2.19998	2.20003	4.81050×10^{-5}
8	2.06635	2.06639	3.45989×10^{-5}
10	1.85664	1.85664	0.00000

The results presented in Table 2 and Figure 8 provide valuable insights into the behavior and properties of the solutions for Eq (1.3) under the specified parameter values. Furthermore, these comparisons demonstrate the effectiveness of our combined analytical and numerical approach in investigating the equations we derived; they also provide evidence of the accuracy and reliability of our numerical and analytical solutions.

Table 3 presents the L_2, L_∞ errors and CPU times for case one at different time levels for Eq (4.4) with the following parameter values: $g_1 = 0.1, g_2 = 0.0001, \nu = 0.01, q = 0.1, R_1 = 0.001, \sigma = 0.001, \vartheta = 0.4, \Delta t = 0.1, \Delta x = 0.2$, and $-10 \leqslant x \leqslant 10$.

Table 3. Results of L_2 and L_∞ errors for case one at different time levels.

t	L_∞-error	L_2-error	CPU time
1	1.18427×10^{-5}	1.74167×10^{-5}	1.248s
3	5.97847×10^{-5}	1.11482×10^{-4}	1.719s
5	9.23073×10^{-4}	2.50966×10^{-4}	2.294s
6	1.61731×10^{-4}	3.45894×10^{-4}	2.327s

From the previous table, it is clear to us that there is stability in the solutions, which means that the method used is effective and good; moreover the time used was minimal, which means that the cost is low.

- **The numerical results for case two: $\lambda = 2, \varrho = 1; p = 2, \rho = 2, \beta = 1, \delta = q^2$**

Table 4 and Figure 9 present a comparison between the numerical results obtained via our numerical scheme and the analytical solution given by Eq (4.12) for Eq (1.3) with the following parameter values: $\Delta x = 0.2$, $\Delta t = 0.1$, $t = 5$, $g_1 = 0.3$, $g_2 = 0.4$, $k = 0.4$, $\nu = 0.001, q = 0.4, -10 \leqslant x \leqslant 10$ and $\sigma = 0.1$.

Table 4. Comparison between the numerical results obtained via our numerical scheme and the analytical solution.

x	Numerical solution	Analytical solution	Absolute error
-10	1.46157	1.46157	0.00000
-8	1.48611	1.48651	4.72781×10^{-4}
-6	1.51075	1.51144	8.31275×10^{-4}
-4	1.53573	1.53635	8.18738×10^{-4}
6	1.66095	1.66125	3.91081×10^{-4}
8	1.68618	1.68634	1.99887×10^{-4}
10	1.71149	1.71149	0.00000

Table 4 and Figure 9 demonstrate how well the numerical and analytical solutions match each other, indicating the accuracy of our numerical scheme and the validity of our analytical solutions.

Table 5 and Figure 10 present a comparison between the numerical results obtained via our numerical scheme and the analytical solution given by Eq (4.13) for Eq (1.3) with the following parameter values: $\Delta x = 0.2$, $\Delta t = 0.1$, $t = 5$, $g_1 = 0.4$, $g_2 = 0.01$, $k = 0.3$, $\nu = 0.1$, $q = 0.001$, $\sigma = 0.001$ and $-10 \leqslant x \leqslant 10$.

Table 5. Comparison between the numerical results obtained via our numerical scheme and the analytical solution.

x	Numerical solution	Analytical solution	Absolute error
-10	3.20432	3.20432	0.00000
-8	3.30431	3.30540	1.09866×10^{-3}
-6	3.37268	3.37348	8.02187×10^{-4}
-4	3.41747	3.41812	6.5164×10^{-4}
4	3.42547	3.42609	6.26715×10^{-4}
6	3.38561	3.38636	7.53512×10^{-4}
8	3.32367	3.32466	1.00123×10^{-3}
10	3.23301	3.23301	0.00000

Table 5 and Figure 10 demonstrate the excellent agreement between the numerical and analytical solutions, confirming the precision of our numerical approach and the soundness of our analytical solutions.

Table 6 presents the L_2, L_∞ errors and CPU times for case one at different time levels for Eq (4.13) with the following parameter values: $\Delta x = 0.2, \Delta t = 0.1, g_1 = 0.4, g_2 = 0.01, k = 0.3, \nu = 0.1$, $q = 0.001, \sigma = 0.001$ and $-10 \leqslant x \leqslant 10$.

Table 6. Results of L_2 and L_∞ errors for case one at different time levels.

t	L_∞-error	L_2-error	CPU time
1	5.94295×10^{-5}	1.38597×10^{-4}	1.063s
3	5.48845×10^{-4}	1.32711×10^{-3}	1.344s
5	1.09866×10^{-3}	3.68560×10^{-3}	2.094s
6	2.10519×10^{-3}	5.28625×10^{-3}	2.116s

Upon analyzing the data presented in the aforementioned table, it becomes apparent that the solutions exhibit a notable degree of stability. This stability indicates that the method employed is not only effective, it is also reliable. Additionally, it is worth noting that the time required to achieve these solutions is relatively minimal, indicating a streamlined and efficient process. Consequently, the low time investment directly translates into reduced costs, further emphasizing the economic viability of the method. Overall, the combination of stability, effectiveness, simplicity, and cost-effectiveness attests to the excellence of the utilized approach.

6. Graphical illustrations

In this study, we employ a combination of analytical and numerical methods to investigate the equations that we have derived. Our objective is to gain a deeper understanding of the system and its dynamics. To facilitate a clear interpretation of our findings, we present a series of two-dimensional and three-dimensional figures that illustrate both the analytical and numerical solutions that we have obtained. The figures presented in this study serve as visual representations of the solutions' behavior. They provide valuable insights into how the system evolves under different conditions as well as shed

light on the influence of various parameters. Specifically, we focus on showcasing the analytical solutions for Eqs (4.3) to (4.13) in Figures 1–6, respectively.

In addition to deriving the analytical and numerical solutions, we also performed a comprehensive evaluation of the accuracy of our numerical scheme and validated the analytical solutions. This evaluation involved comparing the numerical results obtained via our numerical scheme with the corresponding analytical solutions for Eqs (4.3), (4.4), (4.12), and (4.13). Figures 7–10 depict the results of this comparison, showcasing the level of agreement between the numerical and analytical solutions. These figures provide visual representations of the accuracy and validity of our methodologies. By examining the plots in Figures 7–10, we can observe the similarities between the numerical and analytical solutions, indicating that our numerical scheme is capable of accurately approximating the analytical solutions.

It is worth noting that the accuracy of our numerical scheme is demonstrated for various parameter configurations, allowing us to assess its robustness across different scenarios. This analysis further strengthens the validity of our analytical solutions, as the agreement between the numerical and analytical results was found to persist across different parameter settings.

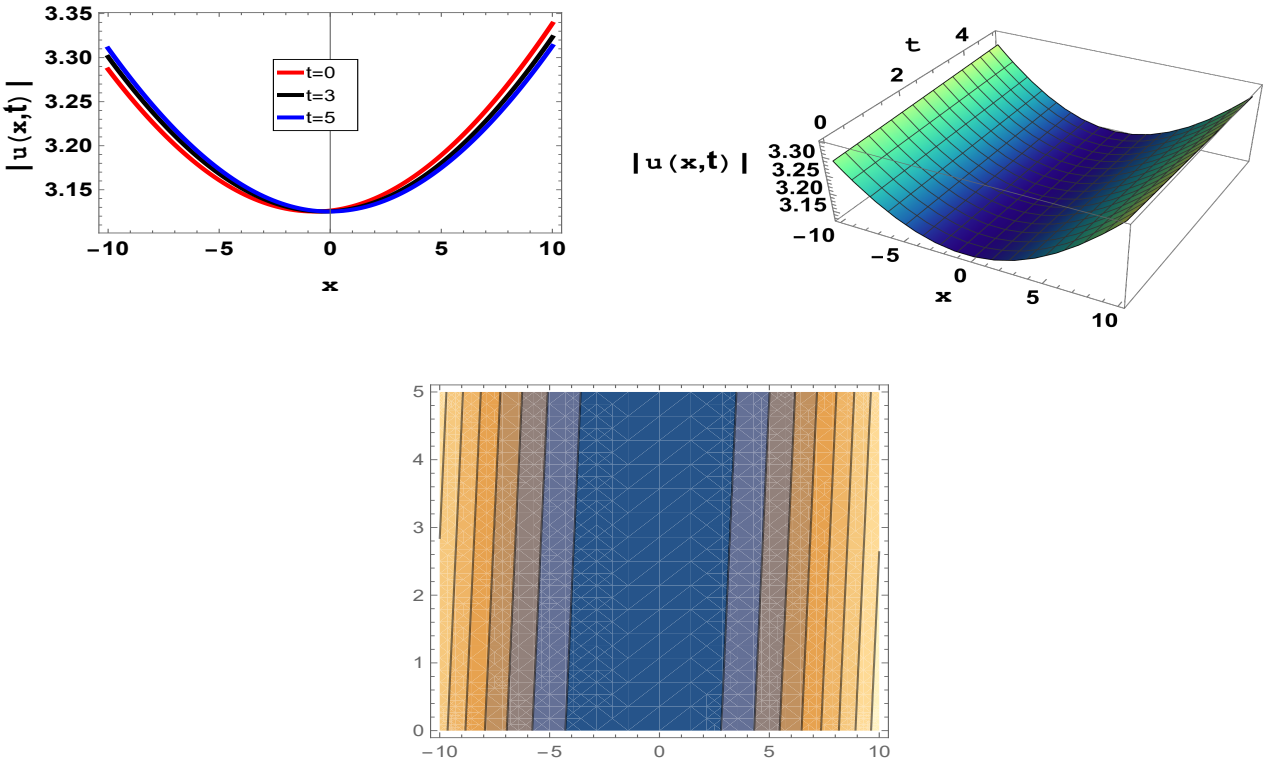

Figure 1. Plots for Eq (4.3) with $g_1 = 0.2, g_2 = 0.01, \nu = 0.001, R_1 = 0.1, \sigma = 0.2, \vartheta = 0.1$.

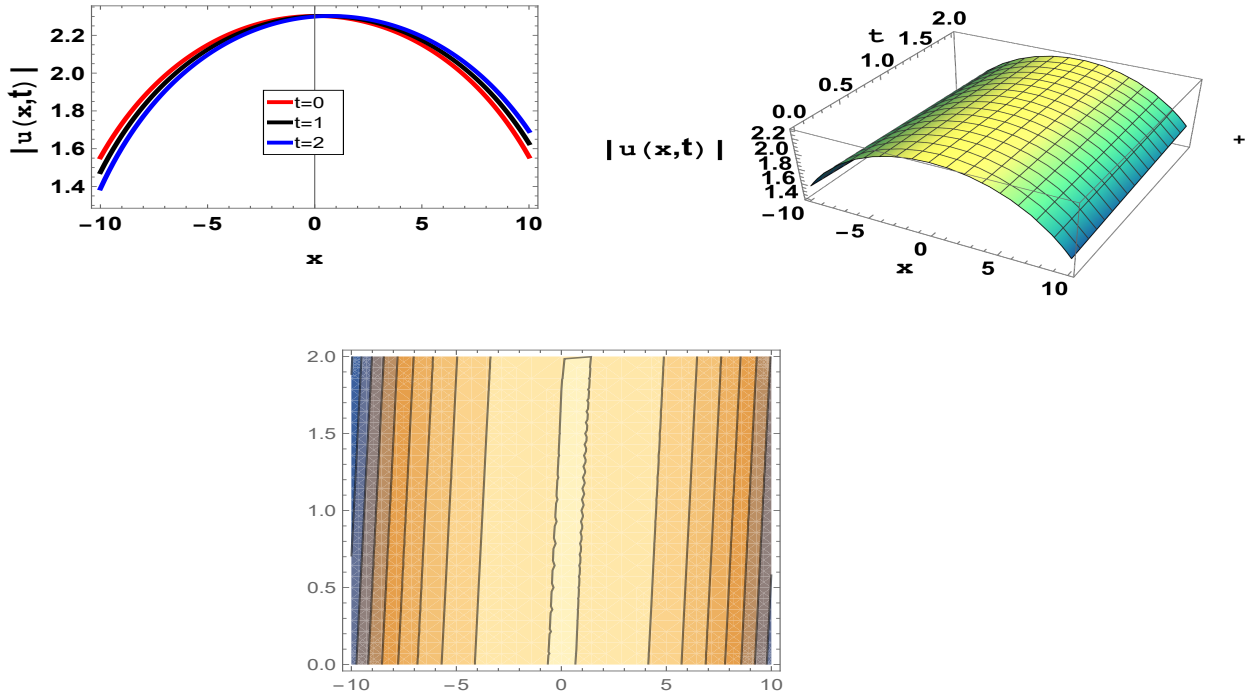

Figure 2. Plots for Eq (4.4) with $g_1 = 0.1, g_2 = 0.0001, \nu = 0.01, R_1 = 0.001, \sigma = 0.001, \vartheta = 0.4$.

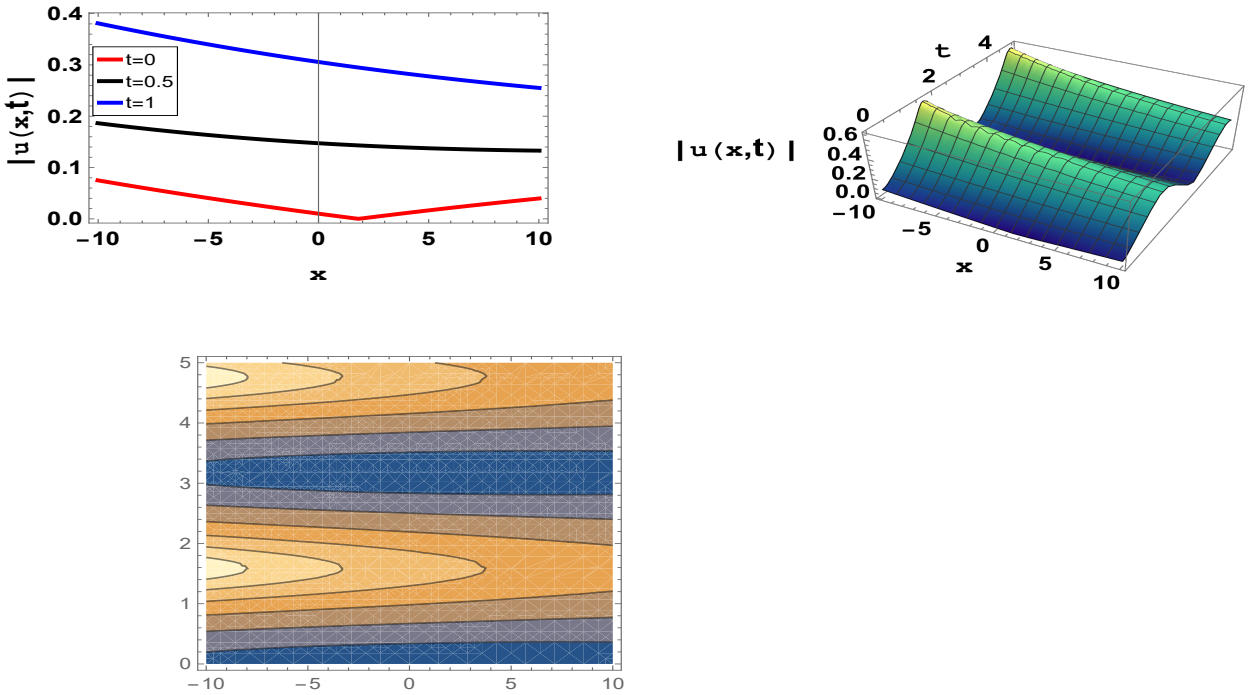

Figure 3. Plots for Eq (4.9) with $g_1 = 0.5, g_2 = 0.2, k = 0.2, \nu = 0.001, \mathfrak{q} = 0.7, \sigma = 0.2$.

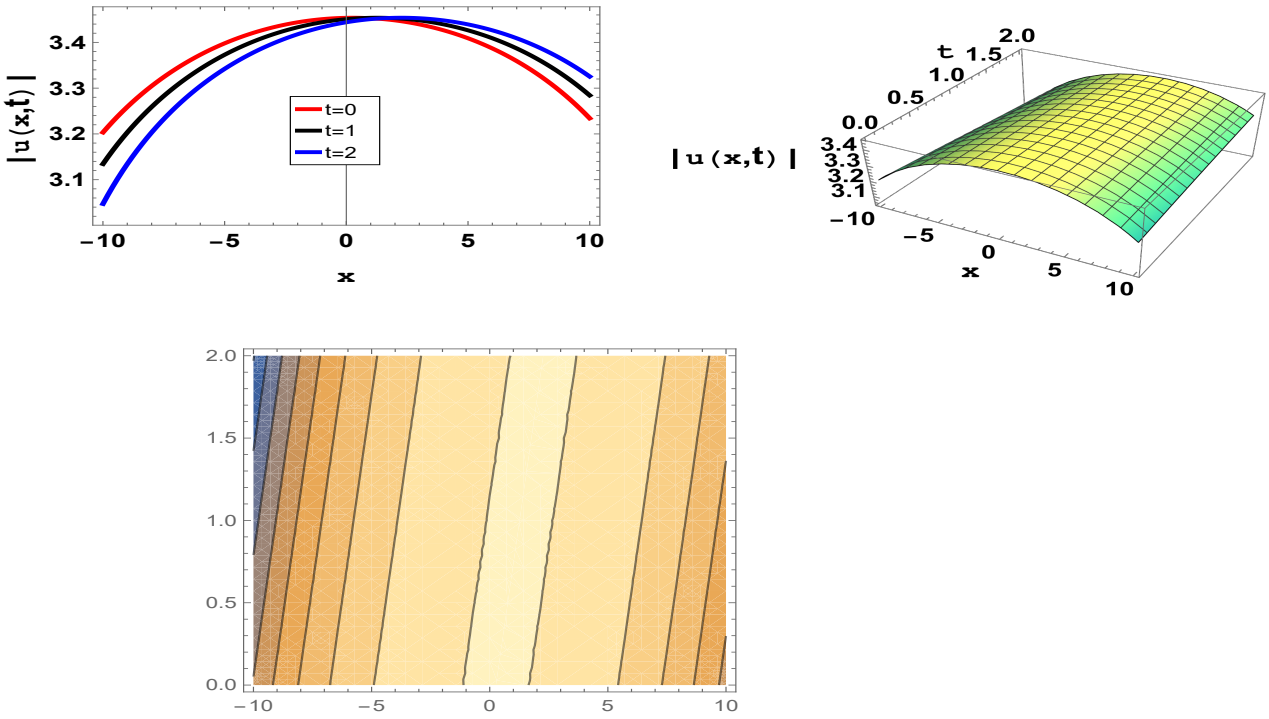

Figure 4. Plots for Eq (4.10) with $g_1 = 0.4, g_2 = 0.01, k = 0.3, \nu = 0.1, \mathfrak{q} = 0.001, \sigma = 0.001$.

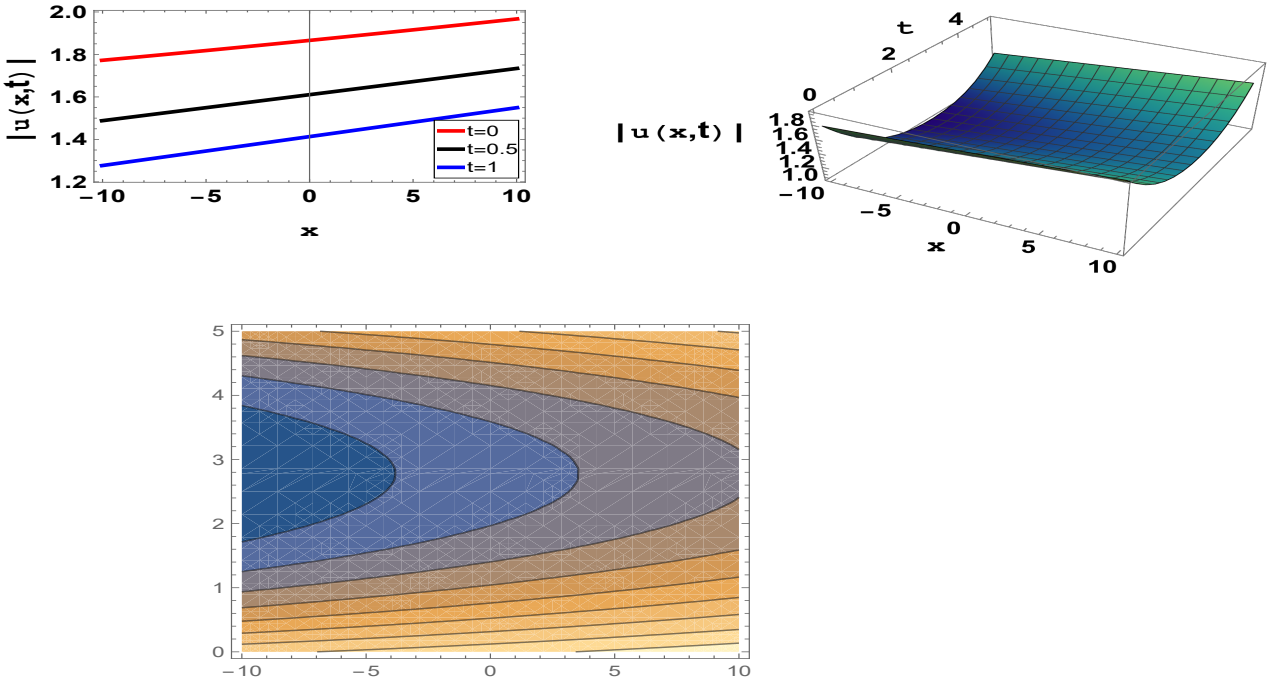

Figure 5. Plots for Eq (4.12) with $g_1 = 0.3, g_2 = 0.4, k = 0.4, \nu = 0.001, \mathfrak{q} = 0.4, \sigma = 0.1$.

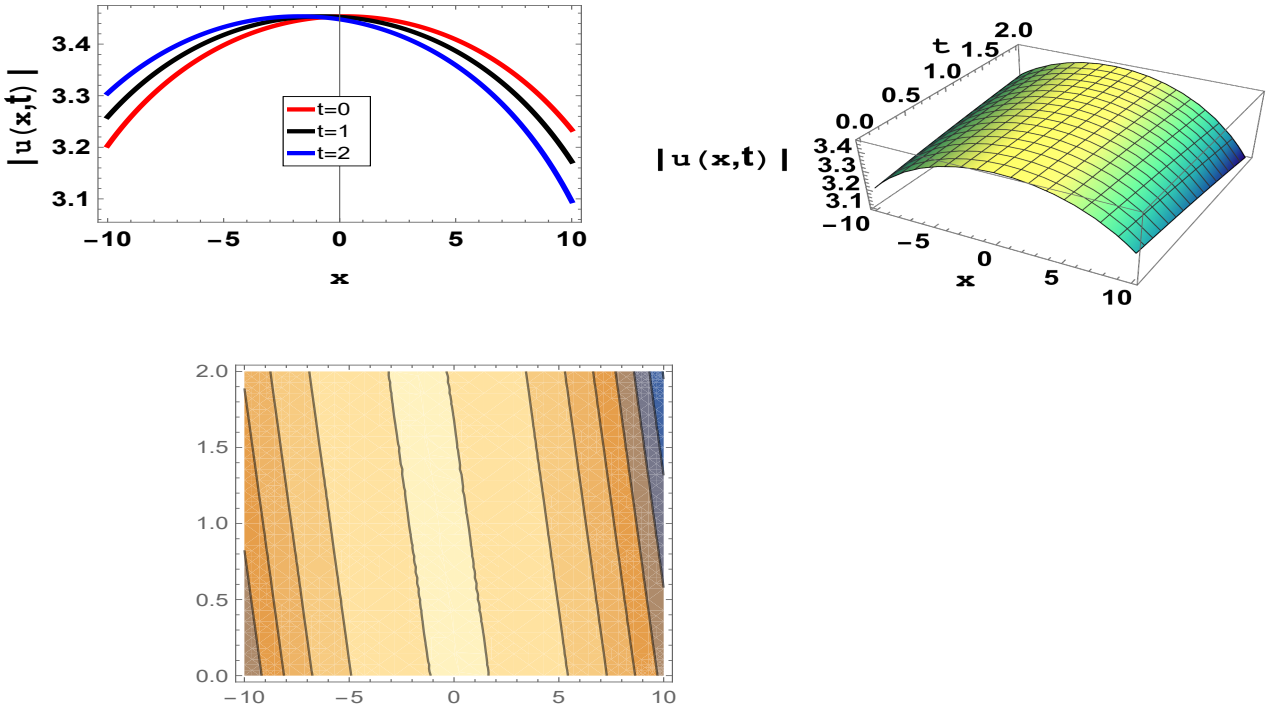

Figure 6. Plots for Eq (4.13) with $g_1 = 0.4, g_2 = 0.01, k = 0.3, \nu = 0.1, q = 0.001, \sigma = 0.001$.

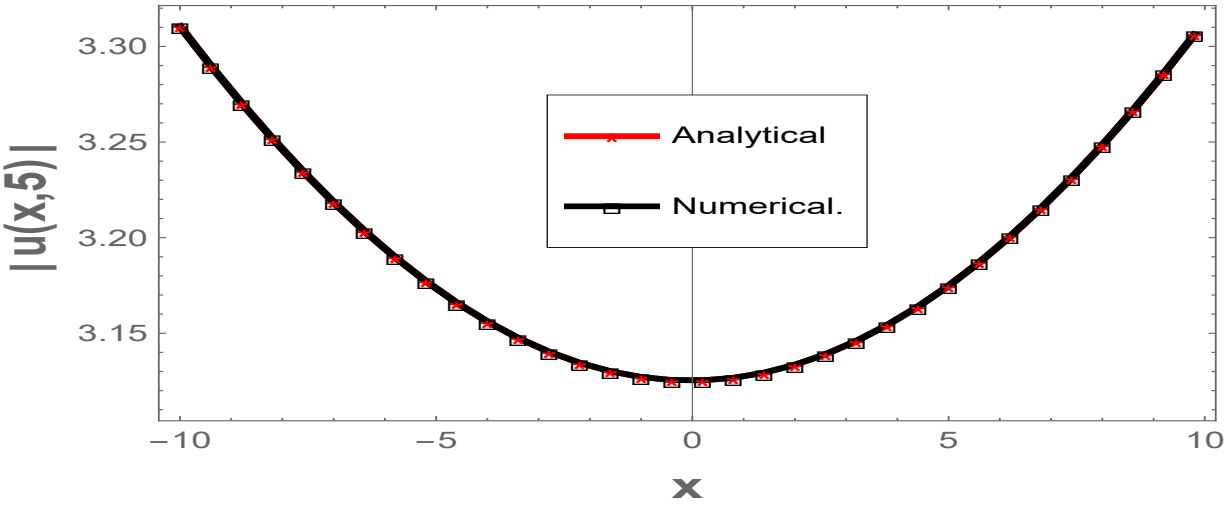

Figure 7. Comparison between the analytical solution of Eq (1.3) and the numerical outcomes for Eq (4.3) with $\Delta t = 0.1, g_1 = 0.2, g_2 = 0.01, \nu = 0.001, \mathfrak{q} = 0.1, R_1 = 0.1, \sigma = 0.2, \vartheta = 0.1, \Delta x = 0.2, t = 5$.

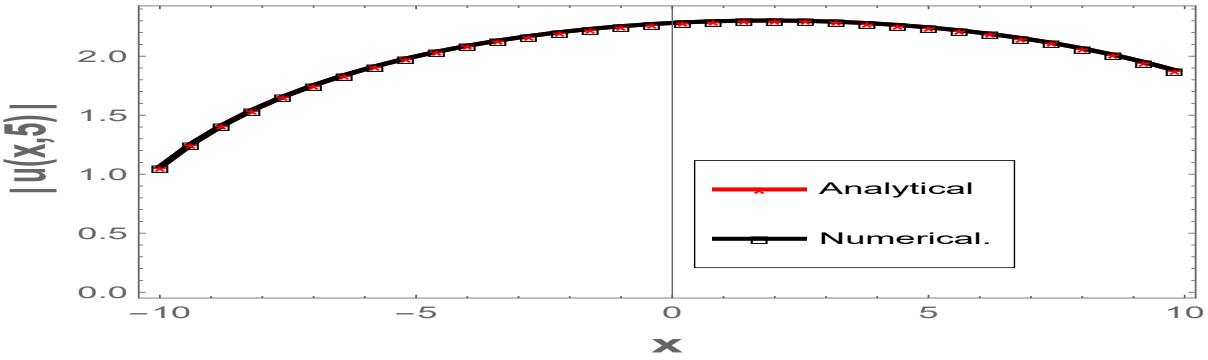

Figure 8. Compare the analytical solution of Eq (1.3) and the numerical outcomes for Eq (4.4) with $g_1 = 0.1, g_2 = 0.0001, \nu = 0.01, \mathfrak{q} = 0.1, R_1 = 0.001, \Delta t = 0.1, \sigma = 0.001, \vartheta = 0.4, \Delta x = 0.2, t = 5$.

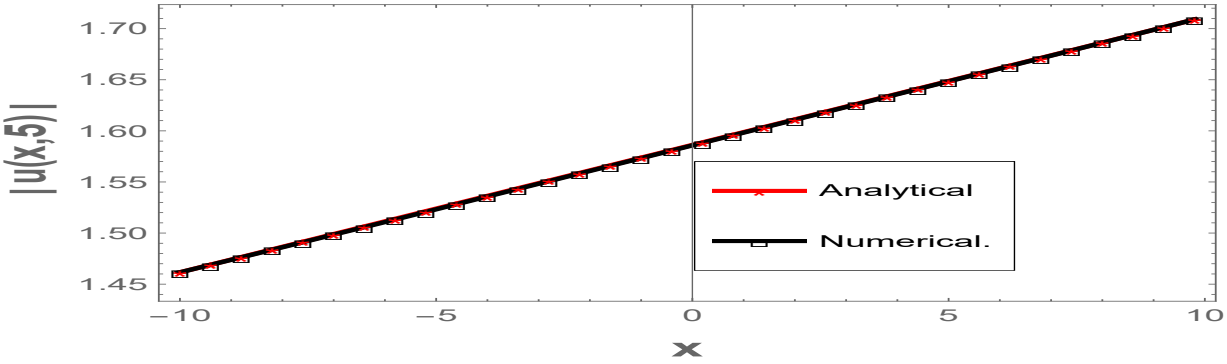

Figure 9. Comparison between the analytical solution of Eq (1.3) and the numerical outcomes for Eq (4.12) with $\Delta x = 0.2$, $t = 5$, $g_1 = 0.3$, $g_2 = 0.4$, $k = 0.4$, $\Delta t = 0.1$, $\nu = 0.001$, $\mathfrak{q} = 0.4$, and $\sigma = 0.1$.

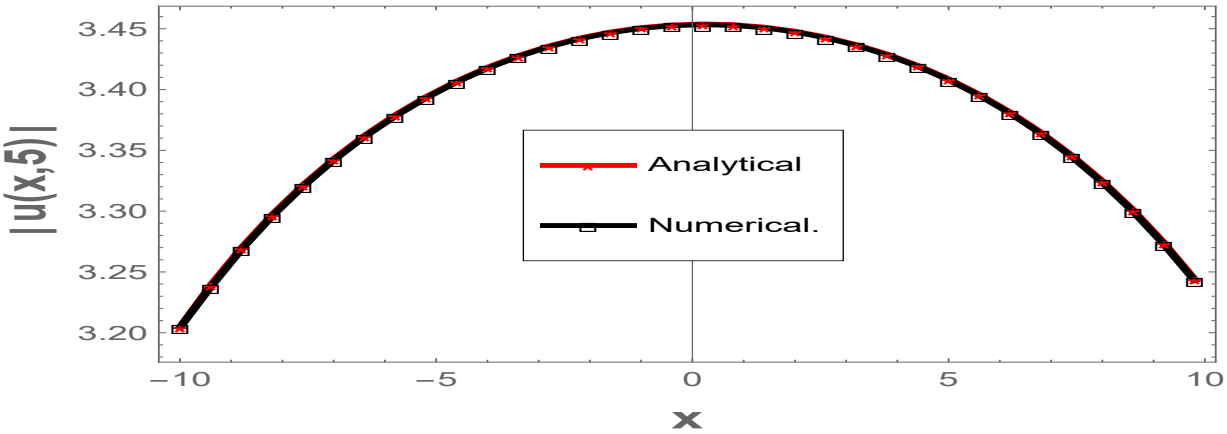

Figure 10. Comparison between the analytical solution of Eq (1.3) and the numerical outcomes for Eq (4.13) with $\Delta t = 0.1, t = 5, g_1 = 0.4, g_2 = 0.01, k = 0.3, \nu = 0.1, \Delta x = 0.2, \mathfrak{q} = 0.001, \sigma = 0.001$.

7. Analysis and discussion

In this paper, we have presented a new form of q-deformed equation (q-deformed tanh-Gordon equation). The analytical and numerical solutions for the q-deformed tanh-Gordon equation are discussed from the perspective of the (G'/G)-expansion method and finite difference method, respectively. Our goal was to compare and contrast the two methods and to demonstrate their effectiveness in solving this nonlinear partial differential equation.

We compared the analytical and numerical solutions and found that they were in good agreement, demonstrating the effectiveness of both methods in solving the q-deformed tanh-Gordon equation. However, we also found that the analytical solutions were significantly faster to obtain than the numerical solutions, but the finite difference method provided a more general solution that could be applied to a wider range of equations.

In conclusion, both the (G'/G)-expansion method and the finite difference method are powerful techniques for solving differential equations, and each has its advantages and disadvantages. The (G'/G)-expansion method can provide analytical solutions that are often expressed in closed form, but may not be applicable to all types of equations. The finite difference method, on the other hand, can provide numerical solutions that are applicable to a wide range of equations, but it may require more computational effort. In the case of the q-deformed tanh-Gordon equation, both methods have been successfully applied to obtain solutions, and the choice of method depends on the specific requirements of the problem at hand. Finally, we see that in Figures 11 and 12, by changing the value of q, the height of the wave varies, becomes distorted and does not maintain its shape, which indicates that the results we have reached are good and can be applied in different fields.

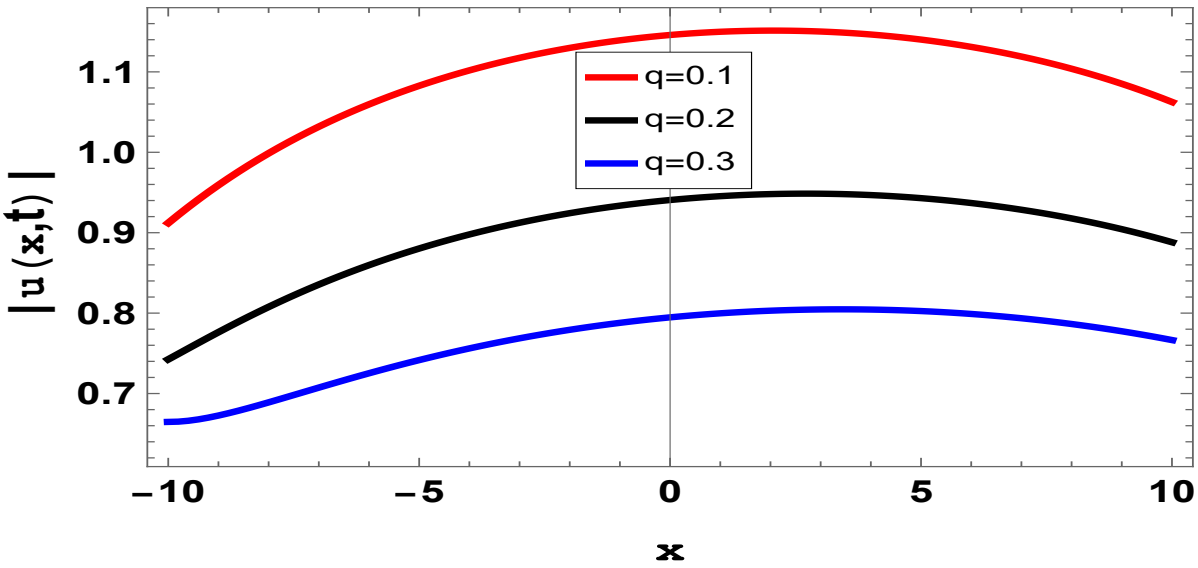

Figure 11. Effects of q parameter on a solitary wave for Eq (1.3) with the numerical outcomes for Eq (4.10) with $g_1 = 0.4, g_2 = 0.01, k = 0.3, \nu = 0.1, t = 2, \sigma = 0.001$.

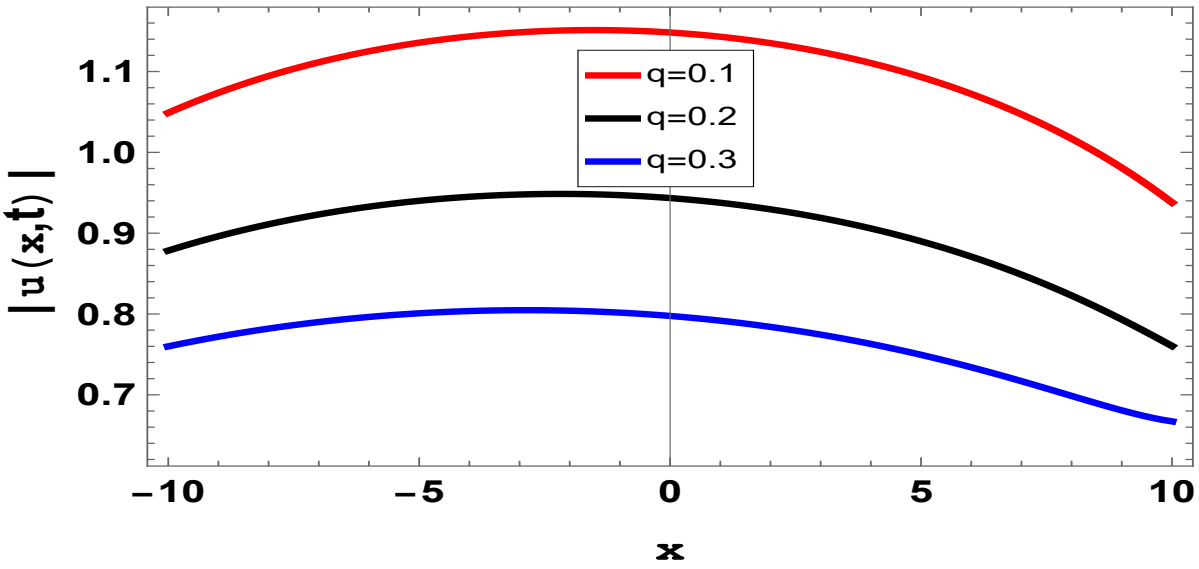

Figure 12. Effecte of q parameter on a solitary wave for Eq (1.3) with the numerical outcomes for Eq (4.13) with $\Delta t = 0.1, t = 5, g_1 = 0.4, g_2 = 0.01, k = 0.3, \nu = 0.1, \Delta x = 0.2, t = 2, \sigma = 0.001$.

Let us go over the physical relevance of these graphical solutions in depth. The study uses the (G'/G)-expansion method to derive solitary wave solutions to the q-deformed problem. The graphical depictions in this section depict various solutions, allowing us to see the system's behavior. Solitary waves are isolated waves that maintain their shape and travel without dispersion. The graphical representations facilitate understanding of the propagation properties of these solitons, such as the amplitudes, widths, and speeds. The graphical depictions show comparisons of analytical and numerical solutions. Visually comparing these solutions allowed us to assess the accuracy and dependability of the analytical approach. Discrepancies or agreements between the two sets of solutions might provide crucial insights into the system's dynamics and the efficacy of the approaches used. Changing the values of the parameters in the q-deformed equation was found to produce different sorts of solutions and different properties. The graphs facilitate determination of the impact of each parameter on the system's behavior, such as changes in waveforms, amplitudes, or speeds. This approach contributes to a better understanding of how q-deformation affects the symmetry and dynamics of physical systems.

8. Conclusions

To summarize, this research constitutes major advances toward understanding of the q-deformed equation, notably the q-deformed tanh-Gordon equation. We have proposed a more generic form of the equation, which broadens the options for modeling physical systems with violated symmetries. We have used the (G'/G)-expansion method to obtain accurate soliton solutions to the q-deformed tanh-Gordon problem. These analytical solutions provide useful information about the system's behavior and dynamics. To validate the analytical results, we applied the finite difference approach to generate numerical solutions for the model. Numerical solutions were derived by discretizing the equation

in space and time, and then iteratively solving the resulting system of algebraic equations. These numerical solutions check the accuracy of the analytical solutions and allow for the investigation of the solution's behavior in more complex settings. We have also included two and three-dimensional tables and illustrations to show comparisons between analytical and numerical solutions. These graphical representations were found to improve the validation process by providing a visual representation of the solution's behavior. The comparisons between the analytical and numerical solutions help to improve overall understanding of the accuracy and dependability of both methods. The $\mathfrak{q}$-deformed tanh-Gordon equation has applications in a variety of domains, including optical physics and quantum mechanics, highlighting its importance as a research topic. This finding has far-reaching implications for prospective applications in quantum computing, making it a hot topic.

Use of AI tools declaration

The authors declare that they have not used artificial intelligence tools in the creation of this article.

Conflict of interest

The authors declare no conflict of interest.

References

1. H. Almusawa, K. K. Ali, A. M. Wazwaz, D. Baleanu, M. S. Osman, Protracted study on a real physical phenomenon generated by media inhomogeneities, *Results Phys.*, **31** (2021), 104933. https://doi.org/10.1016/j.rinp.2021.104933
2. O. Moaaz, H. Ramos, J. Awrejcewicz, Second-order Emden-Fowler neutral differential equations: A new precise criterion for oscillation, *Appl. Math. Lett.*, **118** (2021), 107172. https://doi.org/10.1016/j.aml.2021.107172
3. O. Moaaz, C. Cesarano, A. Muhib, Some new oscillation results for fourth-order neutral differential equations, *Eur. J. Pure Appl. Math.*, **13** (2020), 185–199. https://doi.org/10.29020/nybg.ejpam.v13i2.3654
4. A. Ahmad, R. Ali, I. Ahmad, F. A. Awwad, E. A. A. Ismail, Global stability of fractional order HIV/AIDS epidemic model under Caputo operator and its computational modeling, *Fractal Fract.*, **7** (2023), 643. https://doi.org/10.3390/fractalfract7090643
5. R. Ali, A. S. Hendy, M. R. Ali, A. M. Hassan, F. A. Awwad, E. A. A. Ismail, Exploring propagating soliton solutions for the fractional Kudryashov-Sinelshchikov equation in a mixture of liquid-gas bubbles under the consideration of heat transfer and viscosity, *Fractal Fract.*, **11** (2023), 773. https://doi.org/10.3390/fractalfract7110773
6. R. Ali, E. Tag-eldin, A comparative analysis of generalized and extended (G'/G)-expansion methods for travelling wave solutions of fractional Maccari's system with complex structure, *Alex. Eng. J.*, **79** (2023), 508–530. https://doi.org/10.1016/j.aej.2023.08.007
7. A. Arai, Exactly solvable supersymmetric quantum mechanics, *J. Math. Anal. Appl.*, **158** (1991), 63–79. https://doi.org/10.1016/0022-247X(91)90267-4
8. A. Arai, Exact solutions of multi-component nonlinear Schrödinger and Klein-Gordon equations in two-dimensional space-time, *J. Phys. A-Math. Gen.*, **34** (2001), 4281–4288. https://doi.org/10.1088/0305-4470/34/20/302

9. B. J. Falaye, K. J. Oyewumi, M. Abbas, Exact solution of Schrödinger equation with q-deformed quantum potentials using Nikiforov-Uvarov method, *Chinese Phys. B*, **22** (2013), 110301. https://doi.org/ 10.1088/1674-1056/22/11/110301
10. A. Kurniawan, A. Suparmi, C. Cari, Approximate analytical solution of the Dirac equation with q-deformed hyperbolic Poschl-Teller potential and trigonometric Scarf II non-central potential, *Chinese Phys. B*, **24** (2015), 030302. https://doi.org/ 10.1088/1674-1056/24/3/030302
11. Y. Shu, J. Chen, L. Chen, Bose-Einstein condensation of a q-deformed ideal Bose gas, *Phys. Lett. A*, **292** (2002), 309–314. https://doi.org/10.1016/S0375-9601(01)00816-7
12. S. M. Ikhdair, Rotation and vibration of diatomic molecule in the spatially-dependent mass Schrödinger equation with generalized q-deformed Morse potential, *Chem. Phys.*, **361** (2009), 9–17. https://doi.org/10.1016/j.chemphys.2009.04.023
13. D. Bonatsos, E. N. Argyres, P. P. Raychev, SU-(1,1) description of vibrational molecular spectra, *J. Phys. A-Math. Gen.*, **24** (1991), 403–408. https://doi.org/ 10.1088/0305-4470/24/8/003
14. H. Eleuch, Some analytical solitary wave solutions for the generalized q-deformed Sinh-Gordon equation $\frac{\partial^2 u}{\partial z \partial \mathcal{E}} = [\sinh_q(\beta u^\gamma)]^p - \Lambda$, *Adv. Math. Phys.*, **2018** (2018), 5242757. http://dx.doi.org/10.1155/2018/5242757
15. K. K. Ali, Traveling wave solutions, numerical solutions, and stability analysis of the (2+1) conformal time-fractional generalized q-deformed sinh-Gordon equation, *Nonlinear Eng.*, **13** (2024), 20220348. https://doi.org/10.1515/nleng-2022-0348
16. K. K. Ali, A. Abdel-Aty, H. Eleuch, New soliton solutions for the conformal time derivative q-deformed physical model, *Results Phys.*, **42** (2022), 105993. https://doi.org/10.1016/j.rinp.2022.105993
17. K. K. Ali, N. Al-Harbi, A. Abdel-Aty, Traveling wave solutions to (3 + 1) conformal time derivative generalized q-deformed Sinh-Gordon equation, *Alex. Eng. J.*, **2022** (2022), 1–12, https://doi.org/10.1016/j.aej.2022.10.020
18. K. K. Ali, H. I. Alrebdi, N. A. M. Alsaif, A. Abdel-Aty, H. Eleuch, Analytical solutions for a new form of the generalized q-deformed Sinh-Gordon equation: $\frac{\partial^2 u}{\partial z \partial \mathcal{E}} = e^{\alpha u}[\sinh_q(u^\gamma)]^p - \delta$, *Symmetry*, **15** (2023), 470. https://doi.org/10.3390/sym15020470
19. M. Shallal, K. K. Ali, K. R. Raslan, H. Rezazadeh, A. Bekir, Exact solutions of the conformable fractional EW and MEW equations by a new generalized expansion method, *J. Ocean Eng. Sci.*, **5** (2020), 323–329. https://doi.org/10.1016/j.joes.2019.12.004
20. K. R. Raslan, K. K. Ali, Numerical study of MHD-duct flow using the two-dimensional finite difference method, *Appl. Math. Inf. Sci.*, **14** (2020), 1–5. https://doi.org/10.18576/amis/140417
21. T. S. EL-Danaf, K. R. Raslan, K. K. Ali, New numerical treatment for the generalized regularized long wave equation based on finite difference scheme, *Int. J. Soft Comput. Eng. (IJSCE)*, **4** (2014), 16–24. Available from: `https://www.ijsce.org/wp-content/uploads/papers/v4i4/D2328094414.pdf`.